ACS APPLIED MATERIALS & INTERFACES

www.acsami.org Research Article

Printed, Soft, Nanostructured Strain Sensors for Monitoring of Structural Health and Human Physiology

Robert Herbert, Hyo-Ryoung Lim, and Woon-Hong Yeo*

Cite This: *ACS Appl. Mater. Interfaces* 2020, 12, 25020−25030 Read Online

ACCESS | Metrics & More | Article Recommendations | Supporting Information

ABSTRACT: Soft strain sensors that are mechanically flexible or stretchable are of significant interest in the fields of structural health monitoring, human physiology, and human−machine interfaces. However, existing deformable strain sensors still suffer from complex fabrication processes, poor reusability, limited adhesion strength, or structural rigidity. In this work, we introduce a versatile, high-throughput fabrication method of nanostructured, soft material-enabled, miniaturized strain sensors for both structural health monitoring and human physiology detection. Aerosol jet printing of polyimide and silver nanowires enables multifunctional strain sensors with tunable resistance and gauge factor. Experimental study of soft material compositions and multilayered structures of the strain sensor demonstrates the capabilities of strong adhesion and conformal lamination on different surfaces without the use of conventional fixtures and/or tapes. A two-axis, printed strain gauge enables the detection of force-induced strain changes on a curved stem valve for structural health management while offering reusability over 10 times without losing the sensing performance. Direct comparison with a commercial film sensor captures the advantages of the printed soft sensor in enhanced gauge factor and sensitivity. Another type of a stretchable strain sensor in skin-wearable applications demonstrates a highly sensitive monitoring of a subject's motion, pulse, and breathing, validated by comparing it with a clinical-grade system. Overall, the presented comprehensive study of materials, mechanics, printing-based fabrication, and interfacial adhesion shows a great potential of the printed soft strain sensor for applications in continuous structural health monitoring, human health detection, machine-interfacing systems, and environmental condition monitoring.

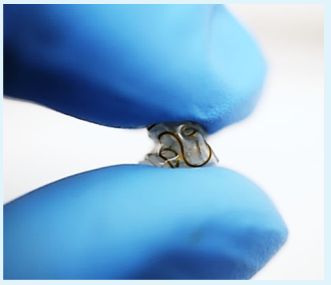

KEYWORDS: *printed strain sensor, soft materials, nanoparticle printing, structural health monitoring, and human physiology monitoring*

Downloaded via GEORGIA INST OF TECHNOLOGY on November 14, 2022 at 21:27:38 (UTC).
See https://pubs.acs.org/sharingguidelines for options on how to legitimately share published articles.

INTRODUCTION

Strain sensors have applications across many areas, including structural monitoring, robotics, environmental science, and human health/motion monitoring.[1,2] With advances in material integration strategies and fabrication techniques,[1,3] numerous thin film strain sensors have been demonstrated with advantages over the conventional rigid strain gauges. Performance of strain sensors is largely determined by the design, materials, and gauge factor (GF; the ratio of the relative change in electrical resistance to the mechanical strain). Although most of the prior works have aimed to optimize these characteristics, there is a lack of studies on other important criteria, such as surface adhesion, wearability, and reusability of sensors.[2,4−13] Both poor adhesion and wearability can significantly lower the sensitivity while preventing continuous, long-term monitoring of strain variation.[14,15]

For structural health monitoring, a strain sensor is often placed on the surface or embedded in the structure to detect strain changes.[9,16−21] Embedding sensors into a structure is not often a feasible integration strategy, especially for large-scale structures.[20] Integrating strain sensors on the surface of a mechanical structure requires a strong, conformal contact to transmit strain to the sensing materials. To accomplish this, many sensors have been fabricated on flexible substrates and attached to the surface via additional tapes or adhesives.[21] An alternative method, but often less feasible, is directly fabricating the sensor on the surface of structures.[9,16,18,19] These existing methods, however, yield poor adhesion and low reusability.

Similar challenges exist for body-wearable strain sensors, where many existing sensors still have rigid components and heavily rely on the use of additional fixtures and/or tapes to mount them on the skin.[12,14,22−24] These supplemental, obtrusive materials detract from patient comfort and limit both wearability and reusability. The need for supporting fixtures is due to poor adhesion and poor conformal contact of the sensor with the skin, which results in the inefficient transfer of strain to the sensor. It has been suggested that the resistance change of strain sensors is affected by the contact area between the sensor and skin.[14,25] To improve the sensor−skin interface, microstructures, hydrogels, and adhesive tapes have been developed, but they require complex, low-throughput fabrica-

Received: March 14, 2020
Accepted: May 12, 2020
Published: May 12, 2020

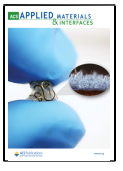

© 2020 American Chemical Society

https://dx.doi.org/10.1021/acsami.0c04857
ACS Appl. Mater. Interfaces 2020, 12, 25020−25030

tion techniques.[14,15,25−28] In particular, a variety of hydrogels have been developed for wearable strain sensing without supporting fixtures.[14,29−31] Such additions to the sensor may be avoided by investigating the interfacial mechanics to ensure conformal contact, which is determined by the study of, including sensor thickness, adhesion, stiffness, and structural patterns. Recent developments in printing techniques[10,18,32−34] have demonstrated different types of fabrication methods using nanomaterials for strain sensors. For example, an aerodynamically focused nanoparticle printer produced strain sensors with high GFs.[35] In addition to deposition printing techniques, lithography-free methods, such as convective self-assembly, chemical surface treatments, and contact printing, have been used to develop wearable strain and pressure sensors with high GFs.[36−38] These sensors, however, still suffer from large feature sizes, complex device mounting steps, and incompatibility with soft material integration.

Here, this work introduces printed, nanostructured strain sensors based on the direct patterning of nanowires and integration with soft materials, with applications in structural health monitoring and human physiology detection. Aerosol jet printing is employed for patterning miniaturized strain sensors and highly stretchable strain sensors. Print parameters and design variations tune sensor resistance, GF, and stretchability. The multilayered printing technique allows for transfer of the ultrathin sensors to soft materials, which provide an adhesive encapsulation to achieve high reusability, conformal contact, and excellent wearability without additional fixtures. Fabricated sensors are applied for both structural monitoring and human health monitoring. A highly flexible, miniaturized strain sensor detects biaxial strain and responds to structural vibrations and impacts. In addition, a highly stretchable strain sensor shows high wearability and unobtrusively detects human motion, pulse, and breathing with a high sensitivity comparable to a clinical-grade system.

RESULTS AND DISCUSSION

Design and Fabrication of Printed Strain Sensors.

Figure 1 summarizes the overview of a printing process for strain sensors and their applications in the detection of human physiology and structural health monitoring. Illustration in Figure 1A shows a wearable, soft strain sensor, mounted on the skin, for monitoring of breathing, pulse, and motion. The ultrathin, nanowire sensor, encapsulated by an elastomeric membrane, enables the conformal contact on the skin across various locations. In addition, the printed soft sensor can be used for structural health monitoring (Figure 1B). The soft and flexible characteristics of the sensor allow for intimate lamination on curved surfaces on a stem valve without the use of additional fixtures. To fabricate these sensors, aerosol jet printing is employed to deposit patterned polyimide (PI) and silver nanowires (AgNWs) onto a glass slide with spin-coated polymethyl methacrylate (PMMA) (Figure 1C; details in Figure S1, the Supporting Information Note S1, and the Experimental Section). The PI ink consists of PI precursor (PI-2545, HD MicroSystems) and solvent (1-methyl-2-pyrrolidinone; NMP, Sigma-Aldrich) in a 4:1 mixture. We followed our prior work to optimize printing of the PI ink.[39,40] The PI ink is atomized via the pneumatic atomizer and deposited through a 300 μm diameter nozzle. The first layer of the PI layer is printed with 4 passes at 10 mm/s and cured for 1 h at 240 °C to achieve a thickness of approximately 3.5 μm and a width of 150 μm (Figure 1D). Print parameters are summarized in Table S1.

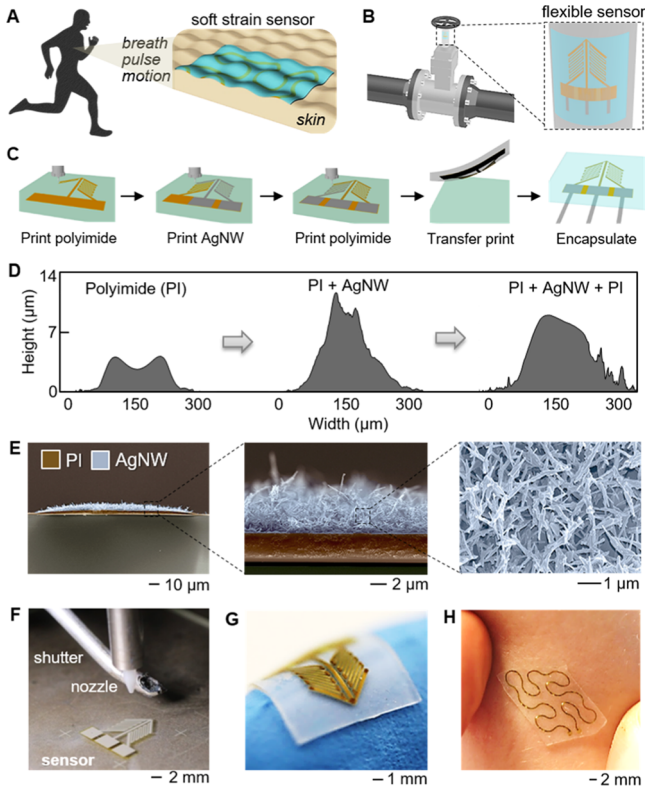

Figure 1. Fabrication of soft strain sensors. (A) Wearable, skin-conformal soft strain sensor for monitoring of breathing, pulse, and motion. (B) Flexible, soft strain sensor, mounted on a stem valve, for structural health monitoring. (C) Fabrication processes, including aerosol jet printing of a polyimide (PI) and AgNW and transfer printing onto a soft material. (D) Profiles of printed layers of a PI-encapsulated AgNW strain sensor. (E) Colorized, cross-sectional scanning electron microscope (SEM) images of a printed AgNW on top of a patterned PI with an enlarged view of the AgNW network. (F) Photo of the utilized printing nozzle, shutter, and printed sensor. (G) Flexible, soft strain sensor mounted on a finger. (H) Wearable soft sensor on the skin, showing no delamination when stretched by fingers.

Prior to depositing AgNWs, the printed PI is plasma-treated to enhance the adhesion of AgNWs to the PI surface. The AgNW layer is then aligned over the PI layer and deposited through a 200 μm diameter nozzle at a speed of 2 mm/s (Video S1). The AgNW ink is a mixture of AgNWs in isopropyl alcohol (IPA) diluted with additional IPA in a 2:1 ratio. The initial suspension is 1% AgNW by weight, and the nanowires have a diameter of 55−75 nm with a length of 20−40 μm. The number of passes controls the sensor's resistance and thickness, where 4 passes yield a thickness of approximately 6.5 μm on top of PI (Figure 1D). Following the printing of AgNWs, the PI ink is aligned and printed again for 4 passes. This top encapsulating layer of PI is observed to integrate with the AgNWs to form a conductive composite and lowers the overall sensor height to approximately 8.5 μm. Curing this top layer of PI at 240 °C for 1 h simultaneously anneals the printed AgNW layer. Thermal annealing of the AgNW network is required to increase conductivity and form a layer with measurable resistance.[8,41−43] Printing AgNWs directly onto the elastomer substrates to eliminate the PI layers would lower bending stiffness and increase GF, but a printed pattern of AgNWs on the elastomer was not conductive without annealing. The PI layers allow for thermal annealing of AgNW layer prior to soft material

https://dx.doi.org/10.1021/acsami.0c04857
ACS Appl. Mater. Interfaces 2020, 12, 25020−25030

integration to avoid damaging the elastomer. Direct printing on the elastomer may be enabled, with future work on alternative nanowire annealing or welding methods compatible with elastomer substrates.[41,43−45] After curing the PI, the glass slide is covered to hold sensors in place and submerged in an acetone bath to dissolve the PMMA layer and allow for transfer of the sensors. Water-soluble tape (ASWT-2, Aquasol) is used to transfer the sensors from the glass slide to elastomer. The elastomer layer is prepared by spin-coating elastomer on a glass slide covered with a sheet of polyvinyl alcohol (PVA). Following transfer, a flexible film cable (heat seal connectors, Elform) is connected to the printed sensors with silver paint (16040-30, Ted Pella), as pictured in Figure S2. Encapsulating with a top layer of the elastomer and removing the underlying PVA layer complete the sensor fabrication. This fabrication process allows for rapid fabrication and modifications of sensors.

The scanning electron microscope (SEM) images in Figure 1E capture the AgNW network on the PI created by the aerosol jet printing. Figure 1F displays the printed sensor after the nozzle was deposited into the AgNW layer and the finalized strain sensor made a conformal lamination on a human finger (Figure 1G). Figure 1H captures a soft wearable sensor being stretched by fingers without delamination. This serpentine design is used for the wearable sensor to achieve conformal contact, similar to wearable, skin-like electronics previously reported.[3,46−48] The conformal contact achieved via the soft encapsulation and ultrathin-printed sensor allows for recording of high-quality signals without the use of additional tapes or bandages.

Optimization and Characterization of Sensor Performance. In this work, we studied the effect of a mechanical pattern on stretchability and variation of GF according to printed passes and pattern dimension. Figure 2A shows the stretchability and GF of a printed stretchable sensor (unit cell of a fractal structure:[49] 11 × 11 mm^2), measured by the change of electrical resistance. This printed sensor uses 1 pass of AgNW. GFs were calculated by fitting a linear curve, where the slope of this curve is the GF

$$\mathrm{GF} = \frac{\Delta R/R}{\epsilon} \tag{1}$$

where ΔR is the resistance change, R is the initial resistance, and ϵ is the strain. GFs were calculated across segmented strain regions of length 25% to show GF at different strain levels (Figure S3).[12,28] The sensor shows a resistance change near 700% at 200% strain with a GF over 13 for strains between 175 and 200%. The resistance change results from the strain developing in the AgNW network of the mesh pattern, which separates and aligns individual AgNWs and reduces the number of junctions along the conductive pathway,[8,50] as illustrated in Figure S4. A resistance change linearity of R^2 = 0.93 is demonstrated from 0 to 100% strain, but decreases to R^2 = 0.53 across 0−200% strain. The nonlinear increase in resistance follows a similar pattern as existing low-density nanowire strain sensors.[8,50−52] Nonlinearity results from the development of bottlenecks in AgNW connectivity, as illustrated in Figure S4. Resistance irregularities at a strain over 175% arise from local delamination between the elastomer encapsulation and the PI/AgNW layers, which results in a temporary reduction of strain on the AgNW network. It should be noted that most existing strain sensors use a bulk, nonpatterned design to achieve higher GF values without stretchability.[2,10,53−56] Even though the mesh-structured strain sensor has lowered GF due to lowered absorbed strain by the AgNW network, this design enables

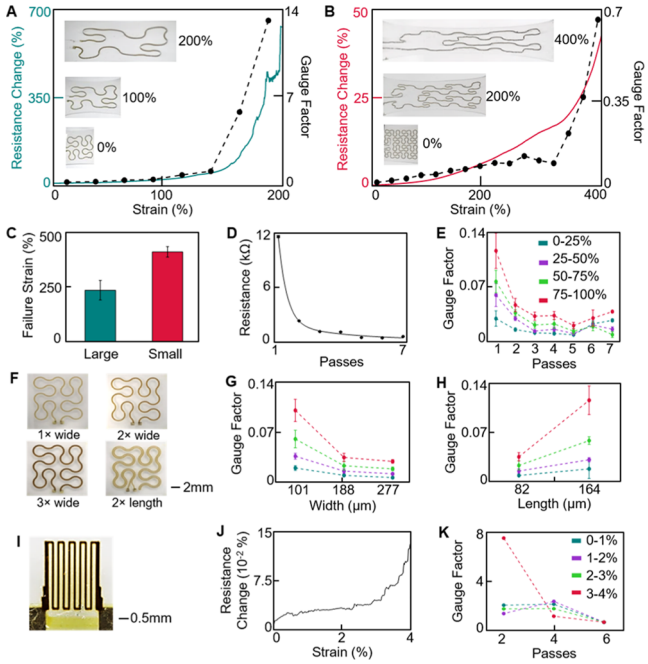

Figure 2. Optimization and characterization of sensor performance. (A) Stretching of a large unit cell strain sensor up to 200% and (B) a small unit cell strain sensor stretching up to 400% with the detection of resistance change and gauge factors. (C) Failure strain of the large and small unit cell strain sensors (n = 3, standard deviation). (D) Decreased resistance with multiple printing passes of AgNW. (E) Increased gauge factor with fewer number of print passes of AgNW. (F) Variations of a sensor design in width and length. (G) Increased gauge factor with a reduced width of a printed sensor. (H) Increased gauge factor with longer sensor pattern. (I) Photo of a printed, flexible strain sensor for sensing low strain change. (J) Resistance change with the strain of flexible strain sensor. (K) Gauge factors for flexible strain sensor while varying the number of AgNW passes.

conformal contact that is critical for on-skin sensor performance and wearability. The mechanical characteristics of patterns can be tuned by the design of a unit cell; more densely packed structure with the same area (Figure 2B) shows an enhanced stretchability. The increased stretchability results in a lower GF, despite also printing 1 pass of AgNW. Figure 2C compares the maximum fracture strain of both patterns in Figure 2 A (large feature) and Figure 2B (small pattern). Error bars show the standard deviation of n = 3. All stretchable sensors in Figure 2 use a two-layered elastomer encapsulation consisting of a 1:2 mixture of Ecoflex 30 and Ecoflex Gel on one side and Ecoflex 30 on the other side. Encapsulation details are discussed in the following section and the Supporting Information Note S1.

In addition to design variations, printing parameters can be used to control the sensor resistance and GF. Prior reports[8,57−59] showed that GF is determined by the density of nanowires; a less dense nanowire network offers a higher GF. The increase in sensitivity for lower density networks is a result of more effective separation of nanowires and fewer conductive pathways through the network.[8,50] The aerosol jet printing, used in this work, offered a precise control of pattern dimension and number of printed passes, which allows for the control of AgNW density. The printing speed was maintained at 2 mm/s with a sensor width of 2 passes while controlling other parameters. Figure 2D shows the drop in sensor resistance for the single unit cell-stretchable sensor from over 1 kΩ to 380 Ω as the number of passes is increased from 1 to 7. The resistivity of the printed

https://dx.doi.org/10.1021/acsami.0c04857
ACS Appl. Mater. Interfaces 2020, 12, 25020−25030

AgNW varies from 1.2 kΩ/cm at 1 pass to 0.046 kΩ/cm at 7 passes (Figure S5A). Due to the resistance and AgNW density variation, the sensors exhibit enhanced GFs for fewer printed passes of AgNW. Figure 2E shows the improvement of the GFs with fewer passes. For each number of passes, GFs are calculated for 25% strain ranges across 0−100% strain. Resistance curves used to calculate these GFs are shown in Figure S5B. GF values are increased according to the applied strain, and a similar trend is determined for the small unit cell sensor (Figure S6).

In addition, the structural dimensions can be modified to control the sensor GF. Figure 2F presents four different dimensions that varied in width and length. All sensors were printed with 2 passes of AgNW. Variation of adjacent printed passes from 1 to 3 makes three different widths, including 101, 188, and 277 μm (Figure 2G), which shows that a smaller width achieves a higher GF. It should be noted that adjacent printed passes are created by printing lines next to each other. Thus, these three sensors use 1−3 adjacent passes, each of which is deposited two times. The decrease in sensitivity with larger widths is due to the overlap of multiple adjacent passes, which increases AgNW density and lowers resistance. Although a narrow trace lowers the strain present in the pattern,[60,61] AgNW density shows a larger impact on sensitivity for this sensor. The original curves for the sensor resistance and change of resistance according to the strain change are shown in Figure S5C,D. Additionally, doubling the sensor length from 82 to 164 μm while maintaining 2 AgNW passes and a 188 μm width shows a significant increase in GF (Figure 2H). The pattern length is increased by duplication of the serpentine pattern inside. This allows strain to be induced at more locations within the pattern. Resistance curves and sensor resistances are shown in Figure S5E,F. To further improve GF of the stretchable strain sensors, less stretchable or higher-density designs may be printed to increase the local strain present in the AgNW layer. Additionally, eliminating the PI layers that mechanically stiffen the AgNW network will allow for larger straining of the AgNW layer and a larger change in resistance. This may be achieved by directly printing a patterned AgNW layer onto the elastomer, but nonthermal nanowire annealing methods need to be investigated to avoid elastomer damage.

The parametric study for a mesh-patterned stretchable sensor is also applicable to a miniaturized strain sensor for structural health monitoring (Figure 2I). For encapsulation, a Silbione layer is applied on one side and Ecoflex 30 on the other side. This strain sensor achieves a maximum stretchability of approximately 4% with a detectable resistance change (Figure 2J). Due to the straight-line design, a GF over 1 is achieved. Similar to the stretchable sensor, varying the number of passes of AgNWs tunes the GF. By using 2 print passes of AgNW, a GF of 2 at low strains (0−2%) and a GF of 7.5 at high strains (2−4%) are achieved (Figure 2K). Corresponding resistance curves are shown in Figure S7. These GFs are comparable to previously reported strain sensors for structural monitoring and that of conventional metallic thin film strain gauges.[11,17,18,32−34,62,63]

Study of Adhesion and Mechanical Behavior of Printed Strain Sensors on Soft Materials. While prior works have focused on GF and stretchability of strain sensors, adhesion and sensor mechanics are not discussed.[4−13] High GF only does not guarantee a sensitive detection of strain changes without sufficient adhesion of sensors on the surface. In this work, we conducted a comprehensive study of a few soft materials and sensor designs for their effects on surface adhesion, modulus, and mechanical reliability upon bending and stretching.

Figure 3A shows an illustration that captures a multilayered strain sensor to make an intimate contact to the surface. The

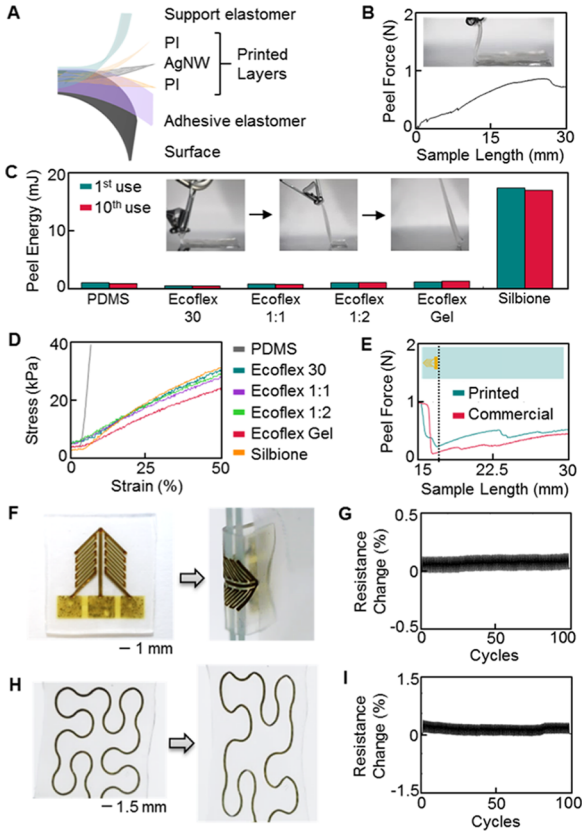

Figure 3. Adhesion and mechanical behavior of printed strain sensors. (A) Illustration of multilayered encapsulation strategy. (B) Peel force, measured along the sample length. (C) Comparison of peel energies for different elastomers at 1st and 10th uses. Photos show the process of peeling from the surface. (D) Stress−strain curves to compare the modulus of different samples. (E) Printed strain sensor shows higher peel force due to increased elastomer surface area resulting from microstructured patterning. (F) Bending of a soft strain sensor around 2 mm diameter edge. (G) Negligible change of resistance during 100 bending cycles (180° bending at 1 mm radius). (H) Stretching (50%) of a wearable strain sensor. (I) Mechanical reliability of the sensor with 100 stretching cycles (50% strain).

support elastomer provides an additional mechanical strength for easy handling of the sensor, while the adhesive elastomer offers higher adhesion to the surface. The thin, unobtrusive layer of adhesive, soft silicone avoids the need for harsher and stiffer adhesives, such as tapes, bandages, and epoxies, which are often added separately to transmit the strain from the surface to the sensor. Figure 3B shows the measured peel force of a 30 mm long sensor from a designated surface. Integration of the area under the peel force curve provides a peel energy for the sample. To determine an optimal substrate, we measured the peel energy with six different types of material compositions in the adhesive elastomer (for details of material preparation, see the Experimental Section and the Supporting Information Note S1). Figure 3C summarizes the result of the measured energies with them, which shows that Silbione substrate offers a significant increase in the peel energy compared to others,

https://dx.doi.org/10.1021/acsami.0c04857
ACS Appl. Mater. Interfaces 2020, 12, 25020−25030

while all elastomers show a minimal change in adhesion after 10 reuses. Details of the values appear in Table S2.

In addition, Figure 3D presents the result of measured Young's modulus of each substrate, showing a similar range in 40−50 kPa, except for the polydimethylsiloxane (PDMS) substrate (∼1 MPa). The previously reported values for a single layer of Ecoflex[64] are well compared to those for multilayered elastomer moduli, indicating a minimal change with two layers of elastomer. Figure 3E compares the peel force between a commercial sensor (062UT, MicroMeasurements) and a printed soft sensor, capturing a larger force drop for the commercial one due to the rigidity of the sensor film despite similar sensor area (Figure S8). To efficiently transmit the strain from the surface to sensor, all structural monitoring sensors and applications use Ecoflex 30 as the support elastomer and Silbione as the adhesive elastomer. For all shown stretchable strain sensors and human health monitoring applications, Ecoflex 30 is used as the support elastomer and a 1:2 mixture of Ecoflex 30 and Ecoflex Gel is used as the adhesive elastomer. Silbione is not required for monitoring on skin due to the low bending stiffness achieved by the serpentine pattern, which more readily allows conformal contact. On skin, the peel energy of the sensor with a 1:2 Ecoflex mixture is similar to that of steel and shows a minor reduction after 10 reuses (Figure S9 and Table S3). As shown in Figure 3F, the highly flexible, soft sensor using the Silbione adhesive elastomer makes an intimate contact (up to 180° bending) on a challenging curved surface (radius: 1 mm). Without using glues or additional fixtures, this sensor would detect a change of low strain due to the conformal contact with enhanced adhesion. The sensor demonstrates a mechanical reliability even with a repeated bending of up to 100 cycles (Figure 3G), where the graph shows a negligible change of resistance. Another example is to manufacture a wearable sensor that has a high stretchability of over 50% (Figure 3H). A cyclic stretching test (100 cycles) in Figure 3I shows a structural safety of this sensor with a minimal change of resistance. This soft sensor also has great flexibility that can endure 180° bending over 100 cycles (Figure S10). With the enhanced mechanics, the soft strain sensors tolerate multimodal, excessive deformations without fracture (Figure S11).

To verify the conformal contact of the strain sensors, an analytical model was developed similar to skin-wearable electrodes.[46,64] The interfacial mechanics relies on sensor bending stiffness, sensor adhesion, and skin roughness. Conformal contact is achieved when the adhesion energy is dominant as follows

$$U_{\text{adhesion}} > U_{\text{bending}} + U_{\text{skin}} \tag{2}$$

where U_{adhesion} is the sensor adhesion energy, U_{bending} is the sensor bending energy, and U_{skin} is the skin elastic energy. In this work, the PI/AgNW/PI sensor structure is modeled as two layers. The first layer is 3.5 μm thick PI and the second is 5 μm thick AgNW/PI composite. The composite layer modulus is determined with a Voigt model, which is used to determine the upper bound of a composite structure's modulus.[65,66] The elastomer encapsulation is 300 μm in thickness. Additional details of the analytical model are provided in the Supporting Information Note S2. The bending stiffness of the wearable sensor is determined to be 3.6×10^{-7} Nm. The bending stiffness depends on the areal fraction of the PI/AgNW pattern, layer thickness, and material moduli. By using a microstructured pattern, the wearable sensor has a low areal fraction of 20%, which is advantageous for a low bending energy. This low areal fraction minimizes the impact of changing PI thickness, AgNW thickness, and the AgNW fill fraction on the bending stiffness (Figure S12). As a result, the elastomer modulus and thickness cause the largest changes in sensor bending stiffness. Figure S13 displays the conformal criteria of the encapsulating elastomer for different areal fractions. If the elastomer properties are above the areal fraction lines, conformal contact is achieved for that sensor pattern and elastomer encapsulation. Additional conformal contact criteria are provided in Figure S14 to demonstrate the effect of sensor parameters on the required work of adhesion. Due to the minor changes in bending stiffness, the minimum work of adhesion to achieve conformal contact shows low variation. Unlike the conventional strain sensors using bulky composite materials, the mesh-patterned sensor in this work lowers the bending stiffness and increases the adhesion energy to achieve conformal contact. For comparison to the patterned sensor, bending stiffness values of example AgNW/PDMS composite sensors are calculated in Figure S15 for different thicknesses and fill fractions. Despite using a 200 μm thickness and 5% fill fraction, the resulting sensor still shows a bending stiffness of 6.7×10^{-7} Nm, which is nearly double that of the sensor in this work. In addition to the conformal contact, the wearable strain sensor enables unobtrusive and comfortable monitoring of human physiological signals. The contact pressure from the sensor−skin contact is defined as

$$\sigma_z = \frac{8\pi^4 E_{\text{skin}} h_{\text{rough}}}{16\pi^3 \lambda_{\text{rough}} + \frac{E_{\text{skin}} \lambda_{\text{rough}}^4}{EI_{\text{sensor}}}} \cos \frac{2\pi x}{\lambda_{\text{rough}}} \tag{3}$$

where h_{rough} and λ_{rough} are the amplitude and wavelength of the skin surface, E_{skin} is the modulus of skin, and EI_{sensor} is the sensor bending stiffness (details in the Supporting Information Note S2).[67] For the printed sensor, the maximum contact pressure is 27 kPa, which is within the sensitivity threshold range for human skin (10−40 kPa).[67−70] Overall, this study reveals the advantages of the soft material-enabled strain sensor with enhanced adhesion and skin conformability.

Flexible Strain Sensor for Structural Health Monitoring. In this study, we demonstrate the functionality of a printed, flexible strain sensor and its application for structural health monitoring on a stem valve. Figure 4A shows a design of biaxial strain gauges that measure the resistance change upon the applied strain in the x and y directions. The nanostructured AgNW precisely measures biaxial strains in a way that the sensor portion in parallel with the applied strain shows over 5 times higher sensitivity than the perpendicular sensor portion. To monitor resistance change, three flexible film cables are used to connect from a multimeter to the three contact pads of the sensor (Figure S2). Connecting the center pad and one outer pad allows for monitoring of a single strain direction. To demonstrate the application for structural health monitoring, the flexible strain sensor is laminated onto a stainless steel stem valve with a radius of 10 mm (Figure 4B), where the impact force is applied to the top surface. A photo in Figure 4C captures the sensor, seamlessly mounted on the curved valve with high adhesion and low bending stiffness. A close-up view of the sensor pattern displays the compact design of printed AgNW patterns. With applied impact forces to the valve, the change of strain is measured by the resistance change.

Figure 4D shows a clear advantage of the printed soft sensor (red line) in sensitivity over the conventional film strain gauge (green line). The change in resistance increases with applied

https://dx.doi.org/10.1021/acsami.0c04857
ACS Appl. Mater. Interfaces 2020, 12, 25020−25030

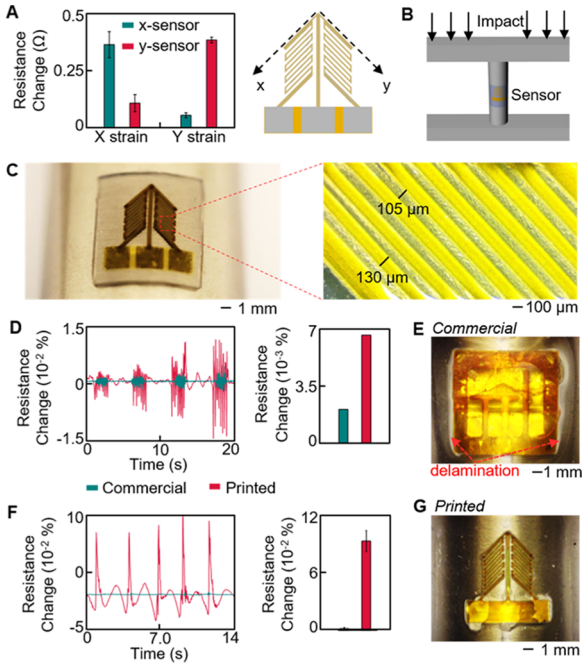

Figure 4. Flexible strain sensor for structural health monitoring. (A) Biaxial strain monitoring via detection of resistance change. (B) Illustration of an experimental setup of a strain sensor on a stem valve that measures strain changes upon the applied impact. (C) Lamination of a flexible sensor onto cylindrical stem valve (left) with an enlarged view of compact AgNW/PI patterns (right). (D) Monitoring of structural vibrations with comparison between printed and commercial strain sensors. (E) Commercial sensor showing delamination at edges due to high bending stiffness. (F) Comparison of the sensitivity between printed and commercial sensors, showing the advantage of the printed sensor. (G) High sensitivity of the printed sensor due to the conformal contact on the stem valve without air gaps.

forces, as indicated by the larger amplitude signals over time (Figure S16). Although both sensors have similar GFs of 2, the enhanced adhesion and conformal contact of the soft sensor provide improved sensitivity due to well-transferred strain from the valve to the sensor. Figure 4E supports the lack of contact quality of the commercial sensor due to delamination at the edges despite using an identical encapsulation material as the soft sensor. This delamination is a result of the high bending stiffness of the sensor and accounts for the decreased sensitivity. This is further exhibited by monitoring individual impacts on the stem valve (Figure 4F). The printed sensor (red line) responds to discrete impacts, while the commercial strain sensor (green line) shows minimal resistance change. Overall, the printed sensor shows 47 times larger sensitivity than the commercial one. A photo in Figure 4G validates a highly conformal contact to the valve surface without sensor delamination, compared to that in Figure 4E. Unlike the stiff commercial sensor, the low bending stiffness of the printed sensor enables self-attachment to more complex surfaces for strain monitoring. Tested samples with different surface shapes include a 45° angle, concave and convex 90° angles, and a conical shape (Figure S17). Another advantage of the printed sensors is reusability, showing no degradation of sensitivity over reuses 20 times (Figure S18). Depending on a surface geometry, another sensor with a fractal pattern can be used for strain sensing (Figure S19).

Table 1 compares the aerosol jet-printed soft strain sensor with prior works that show printed strain sensors for structural health monitoring. The sensor used for comparison in Table 1 is the uniaxial sensor shown in Figure 2I to allow for comparison with the existing uniaxial strain sensors. The uniaxial sample is equivalent to half of the biaxial sensor. In addition to these structural strain sensors, an aerodynamically focused nanoparticle printer has previously produced strain sensors with mechanical cracking to achieve GFs over 290.[35] Our sensor using a soft elastomeric encapsulation shows the first demonstration of reusability during strain sensing with a small feature size and reasonable GF. Although it has been reported that embedding strain sensors in soft materials results in stiffening and reduction of measured GF, the printed sensors introduced here achieve high sensitivity due to the enhanced sensor−surface interface.[71,72]

Stretchable Strain Sensor for Human Physiology Monitoring. Soft, stretchable strain sensor, developed in this work, offers conformal lamination on the deformable skin, which enables a number of possible applications in human health monitoring, motion detection, and human−machine interfaces.[3,46,73] Table 2 captures the advantages of the printed soft strain sensor we developed, compared to those of the other printed wearable sensors for human health monitoring. The stretchable sensor shown in Figure 2A is used for comparison

Table 1. Comparison of Printed Strain Sensors for Structural Health Monitoring

ref (year)	method	material	substrate	reusability	feature size (μm)	sensor area (mm²)	max strain (%)	GF
this work	AJP[a]	AgNW	elastomer	yes	t: 9 w: 150	4 × 5 or 2.4 × 3	4	1−7.5
32 (2018)	AJP	AgNP[b]	H-cement[c]	no	t: n/a w: 68	2 × 6.5		3.15
33 (2019)	AJP	AgNP	CNT sheet[d]	no	t: n/a w: 400			0.5−1.7
18 (2019)	AJP	AgNF[e]	PVC tube[f]	no	t: 8 w: 160			1.04
34 (2017)	inkjet	AgNP	PET[g]	[h]	t: 2 w: 180		1	3.7
34 (2017)	screen	carbon paste	PET		t: 18 w: 340		1	8.8
17 (2017)	screen	CB[i]/CNT	PDMS[j]	no	t: 8000 w: 15 000	8 × 15	25	12.25
11 (2017)	screen	graphite silver CNT[k]	PEN[l]	no	t: n/a w: 150		0.05	1.2−6.68
16 (2017)	AFN[m]	AgNP	PE/PI/plastic[n]	no	t: n/a w: 65		1	5−30
63 (2017)	fluid dispensing[o]	carbon paste	PET	no	t: n/a w: 225	3 × 6		59

[a]AJP: aerosol jet printing. [b]AgNP: silver nanoparticles. [c]H-cement applied onto the cantilever beam prior to printing the sensor onto a beam. [d]CNT: carbon nanotube. [e]AgNF: silver nanoflakes. [f]PVC: polyvinyl chloride. [g]PET: polyethylene-terephthalate. [h]Strain sensors were not applied for structural monitoring, and the method of attachment is not provided. [i]CB: carbon black. [j]PDMS: polydimethylsiloxane. [k]Three different inks are tested. [l]PEN: polyethylene-naphthalate. [m]AFN: aerodynamically focused nanoparticle printer that uses solvent-free nanoparticles. [n]PE: polyethylene, PI: polyimide; other plastics include carbon- and glass-reinforced plastics. [o]A pressurized syringe deposited carbon paste onto a movable stage.

https://dx.doi.org/10.1021/acsami.0c04857
ACS Appl. Mater. Interfaces 2020, 12, 25020−25030

Table 2. Comparison of Printed Wearable Strain Sensors for Human Health Monitoring

ref (year)	printing method	material	skin mounting method	feature size (μm)	sensor area (mm^2)	max strain (%)	GF
this work	AJP	AgNW/Ecoflex	device itself (no additional material)	t: 9 w: 150	11 × 11	400	0.1
4 (2015)	drop-cast/pen-writing[a]	AuNW/Latex	added glove	t: 2 w: 5000	8 × 30	150	13
5 (2014)	embedded fluid dispensing[b]	carbon grease/Ecoflex	added glove	n/a[c]	4 × 20	450	3.8
6 (2015)	fluid dispensing[d]	AgNW/PDMS	n/a[e]	w: 500		60	5
24 (2019)	AJP	AgNP/polyurethane	added skin tape[f]	t: 1 w: 200	9 × 10		
12 (2019)	3D printing[g]	graphene/PDMS	added skin tape			350	18
13 (2018)	spray deposition	CNT/PDMS	added skin tape	t: 8.4	15 × 20	45	36
28 (2017)	3D printing[h]	hydrogel/tape	added skin tape			1000	0.6

[a]Gold nanowire ink was drop-casted or deposited by hand-drawing with a penbrush. [b]Ink was deposited by placing a deposition nozzle into an elastomer and moving it. The nozzle forms an empty reservoir as it moves, which is filled by ink flowing out of the nozzle. [c]Cross-sectional area was measured to vary from 0.066 to 0.71 mm^2 depending on the printing speed. [d]A dispensing nozzle printer was used, where ink was deposited through a needle. [e]Skin mounting method was not shown or discussed. [f]Sensor printed onto a commercial bandage consisting of polyurethane and an acrylic adhesive. [g]Extrusion-based three-dimensional (3D) printing with a biological 3D printer was used to print graphene−PDMS ink. [h]A 3D bioprinter was used to print hydrogel ink.

and for human health monitoring. This work shows the direct mounting of a stretchable strain sensor on the skin, without using additional fixtures or tapes, for highly sensitive detection of physiological signals. To attach the sensor to the skin, the sensor was laminated on the skin and gently pressed to ensure all edges contact the skin. The thin and adhesive sensor package maintains contact by itself, via van der Waals interactions, throughout movements and skin deformation.

Figure 5A displays photos showing the printed soft strain sensor, seamlessly mounted on the skin, which maintains the conformal contact even with excessive wrinkling of skin. The fractal-structured sensor can endure multimodal deformation, including biaxial strain over 100% without fracture (Figure 5B). The ultrathin, soft, skin-conformal sensor shows an extremely small form factor, as demonstrated in Figure 5C. The finger-worn application compares the size advantage compared to a miniaturized integrated circuit (IC) chip. Even with 90° bending of the finger, the sensor maintains a highly conformal contact on the finger joint without additional fixtures, which can successfully detect subtle changes of the bending angle via recording of electrical resistance (Figure 5D; n = 3, standard deviation). Details of electrical resistance data for each bending angle are provided in Figure S20. In all monitoring applications, flexible film cables are attached to connect the open ends of the serpentine pattern to a multimeter (Figure S2).

In addition, the wearable strain sensor enables human health monitoring via detection of pulse waves and breathing patterns on the skin. Figure 5E shows a photo of the stretchable sensor mounted on the wrist for the detection of pulse. Without additional tapes or applied pressure, the skin-wearable sensor clearly measures the change of electrical resistance as the radial artery pressure applies strain to the skin. The recorded pulse wave's morphology is in agreement with the previous studies of wrist pulse monitoring.[12,74] To validate the pulse wave, photoplethysmogram (PPG) and oxygen saturation (SpO_2) are simultaneously obtained by using a commercial, clinical-grade device (BioRadio, Great Lakes NeuroTechnologies; Figure 5F). The two signals show similar morphologies, which corresponds with previous reports.[75] An enlarged view of an individual pulse in Figure 5G captures both P-wave and D-wave from both sensors. The detection of the subtle strain changes on the wrist from pulses highlights the importance of adhesion and conformal contact for wearable strain sensor performance.

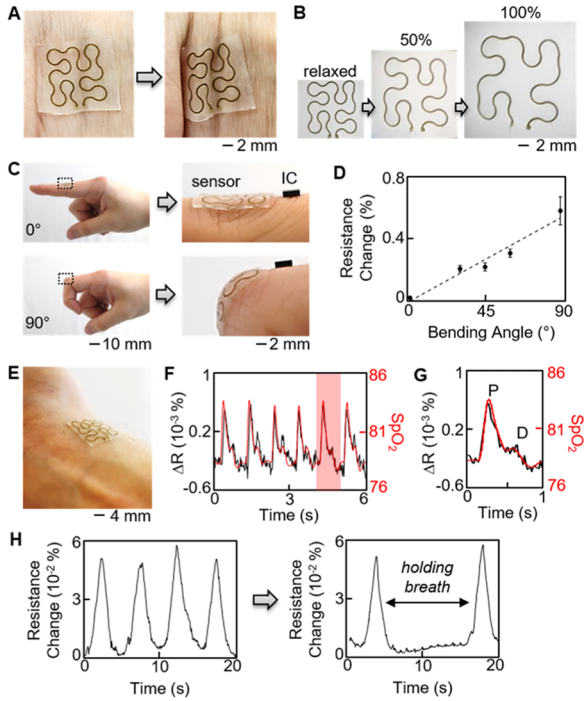

Figure 5. Stretchable strain sensor for human physiology monitoring. (A) Stretchable sensor on the skin, maintaining an intimate contact despite wrinkling. (B) Photos of a stretchable sensor showing 100% biaxial stretchability without fracture. (C) Comparison of the size and conformal lamination of the sensor on the index finger with a small integrated circuit (IC) chip. (D) Highly sensitive detection of a finger-bending motion with the strain sensor on the skin. (E) Photo of the strain sensor on the wrist for monitoring of pulse. (F) Comparison of the measured oxygen saturation (SpO_2) from a commercial sensor (BioRadio; red line) to resistance change from the strain sensor (black line). (G) Magnified view of an individual pulse where the strain sensor (black line) clearly captures the P-wave and D-wave, validated by SpO_2 signal morphology. (H) Sensitive detection of breathing rate with the strain sensor, mounted on a subject's upper abdomen. Graph on the right captures the change of breathing rate when the subject briefly held a breath.

Additionally, the strain sensor is able to detect a subject's breathing rate when laminated on the upper abdomen (Figure 5H).

https://dx.doi.org/10.1021/acsami.0c04857
ACS Appl. Mater. Interfaces 2020, 12, 25020−25030

CONCLUSIONS

This paper reports two types of printed, soft, nanostructured strain sensors for the highly sensitive detection of force-induced strain on a mechanical structure and human physiological signals on the skin. The ultrathin, low-profile sensors, fabricated by a high-throughput printing method, demonstrate an enhanced adhesion, multiple reusability, and excellent wearability. A printed, two-axis strain gauge, mounted on a metal stem valve, shows an enhanced gauge factor, improved contact quality, and reusability, compared to a commercial strain film sensor. A stretchable, soft wearable strain sensor that is laminated on the skin (finger, wrist, and abdomen) proves the functionality of the device in a highly sensitive detection of finger-bending motion, pulse, and breathing rate, which is validated by comparing the data with a clinical-grade device. Future studies will focus on the integration of the soft sensors with soft, wireless nanomembrane circuits for applications in portable, continuous human health monitoring and persistent structural health management.

EXPERIMENTAL SECTION

Fabrication of Soft Strain Sensors. An aerosol jet printer (Optomec 200; Optomec Inc.) deposited sensor layers. PMMA was spin-coated on a cleaned glass slide at 3000 RPM for 30 s and baked at 180 °C for 3 min. PI ink consists of a 4:1 mixture of PI-2545 precursor and NMP and was placed in the pneumatic atomizer. PI was deposited with 4 passes at a speed of 10 mm/s with a 300 μm nozzle diameter. The substrate was heated to 80 °C during printing. Printed PI was cured at 240 °C for 1 h. Before printing AgNW, the printed PI was plasma-treated for 30 s. AgNW ink consisted of AgNWs mixed with IPA and was placed in the ultrasonic atomizer with a water temperature of 27 °C. A 200 μm nozzle printed AgNWs at the set number of passes at 2 mm/s while the substrate was heated to 80 °C. A top PI layer was printed with identical conditions as the first PI layer and then cured at 240 °C for 1 h. Next, the PMMA layer was dissolved in an acetone bath to allow for transfer of the sensors. Elastomer was prepared by mixing Ecoflex 30 in a 1:1 ratio of Parts A and B; Ecoflex Gel in a 1:1 ratio of Parts A and B; and Silbione in a 1:1 ratio of Parts A and B. Ecoflex 30 and Gel combinations were created by mixing the two elastomers separately in their 1:1 ratios before combining together in a 1:1 or 1:2 ratio of Ecoflex 30 to Gel. PDMS was prepared by mixing in a 10:1 ratio of base to cure. All elastomers were spin-coated at 500 RPM onto the PVA film. After transfer with a water-soluble tape, flexible film cables were attached with silver paint. Encapsulation was completed by adding the "supporting" elastomer over the sensor. Additional details are provided in the Supporting Information Note S1.

Strain Sensor Stretching and Bending. To stretch strain sensors, a motorized test stand (ESM303, Mark-10) was used to stretch samples to a set distance. Samples were clamped at the top and bottom for attachment to the test stand. A multimeter (DMM7510; Keithley) recorded resistance changes during stretching. Cyclic stretching was performed by setting the number of cycles to 100. Cyclic bending was performed by attaching sensors to joined glass slides that bent from 0 to 180° when the test stand was operated.

Peel Force and Modulus Measurement. Peel force and modulus measurements were completed with the motorized test stand (ESM303, Mark-10) and a force gauge (M5-5, Mark-10). Elastomer samples were prepared to have a 40 mm length, 15 mm width, and 0.5 mm thickness. To record the peel force, one end of the elastomer sample was clamped to allow for a 30 mm length of the elastomer to be laminated to a stainless steel sheet. The motorized test stand then pulled the elastomer sample from the clamped end, while the force gauge recorded the applied force until the elastomer was detached. Peel energy was determined by integrating the peel force over the length of the sample. For modulus, the elastomer sample was clamped on both ends and stretched to 50%. A linear fit was determined across the stress–strain curve, and the slope was the modulus.

Structural Monitoring with Stem Valve. Strain sensors were laminated on a stainless steel stem valve. The stem valve was fixed in place while a force from a hammer or hand was applied at the top of the stem valve along the length of the valve. For comparison with the printed strain sensor, a commercial sensor (062UT, MicroMeasurements) was used. A high-pass filter with a cutoff frequency of 0.5 Hz was applied to remove baseline drift and noise resulting from wire motion artifacts.

Wearable Sensor Monitoring and Validation. Wearable sensors were laminated on skin without additional tapes for strain monitoring. For validation of the measured wrist pulse, PPG was simultaneously recorded and compared with a clinical-grade, commercial device (BioRadio, Great Lakes NeuroTechnologies). The resistance signal for monitoring the wrist pulse was filtered using a high-pass filter with a cutoff frequency of 1 Hz to remove wire motion artifacts.

Recording of Physiological Signals. We completed a set of experiments with one human subject to validate the performance of the wearable strain sensor. The noninvasive monitoring of physiological signals was conducted at Georgia Tech (IRB# H17212). Prior to the experiments, this participant provided written informed consent.

ASSOCIATED CONTENT

Supporting Information

The Supporting Information is available free of charge at https://pubs.acs.org/doi/10.1021/acsami.0c04857.

Note S1: fabrication of printed strain sensors; Note S2: analytical model for conformal contact and contact pressure; Figure S1: fabrication steps for printed strain sensors; Figure S2: strain sensor wiring using silver paint to attach flexible film cables; Figure S3: illustration of GF calculation; Figure S4: illustration of strain-sensing mechanism; Figure S5: resistance change with strain for printed strain sensor designs; Figure S6: gauge factor tuning via passes for small unit cell sensor; Figure S7: resistance change with strain for flexible sensor; Figure S8: photos of commercial and soft strain sensors; Figure S9: adhesion between sensor and skin; Figure S10: cyclic bending of stretchable sensor; Figure S11: large deformations of strain sensors; Figure S12: effect on sensor bending stiffness of different sensor parameters; Figure S13: conformal contact criteria for printed sensor; Figure S14: effect on adhesion required for the conformal contact of sensor parameters; Figure S15: estimated bending stiffness of a sensor using a PDMS–AgNW composite; Figure S16: force sensitivity of flexible sensor; Figure S17: printed strain sensor laminated on various surface geometries; Figure S18: average resistance change of sensor during impacts after multiple reuses; Figure S19: stretchable sensor for structural monitoring; Figure S20: resistance signals from bending finger; Table S1: printing parameters for PI and AgNW; Table S2: peel energy and modulus of elastomers; and Table S3: peel energy of sensor from a steel surface and skin (PDF)

Video S1: printing of AgNW for fabrication of a strain sensor (MP4)

AUTHOR INFORMATION

Corresponding Author

Woon-Hong Yeo – *George W. Woodruff School of Mechanical Engineering, Institute for Electronics and Nanotechnology and Wallace H. Coulter Department of Biomedical Engineering, Georgia Institute of Technology, Atlanta, Georgia 30332, United States; Parker H. Petit Institute for Bioengineering and Biosciences, Neural Engineering Center, Institute for Materials,*

https://dx.doi.org/10.1021/acsami.0c04857
ACS Appl. Mater. Interfaces 2020, 12, 25020–25030

Institute for Robotics and Intelligent Machines, Georgia Institute of Technology, Atlanta, Georgia 30332, United States; orcid.org/0000-0002-5526-3882; Email: whyeo@gatech.edu

Authors

Robert Herbert − *George W. Woodruff School of Mechanical Engineering, Institute for Electronics and Nanotechnology, Georgia Institute of Technology, Atlanta, Georgia 30332, United States*

Hyo-Ryoung Lim − *George W. Woodruff School of Mechanical Engineering, Institute for Electronics and Nanotechnology, Georgia Institute of Technology, Atlanta, Georgia 30332, United States;* orcid.org/0000-0002-0828-2853

Complete contact information is available at: https://pubs.acs.org/10.1021/acsami.0c04857

Author Contributions

R.H. and W.-H.Y. conceived and designed the research; R.H. conducted the analytical and experimental research; R.H., H.L., and W.-H.Y. analyzed the data; and R.H., H.L., and W.-H.Y. wrote the paper.

Notes

The authors declare the following competing financial interest(s): Georgia Tech has a pending US patent application regarding the presented work in this paper.

■ ACKNOWLEDGMENTS

W.-H.Y. acknowledges the support from the American Heart Association (grant 19IPLOI34760577) and from the Institute for Electronics and Nanotechnology, a member of the National Nanotechnology Coordinated Infrastructure, which is supported by the National Science Foundation (grant ECCS-1542174).

■ REFERENCES

(1) Herbert, R.; Kim, J.-H.; Kim, Y. S.; Lee, H. M.; Yeo, W.-H. Soft material-enabled, flexible hybrid electronics for medicine, healthcare, and human-machine interfaces. *Materials* **2018**, *11*, 187.

(2) Amjadi, M.; Kyung, K. U.; Park, I.; Sitti, M. Stretchable, skin-mountable, and wearable strain sensors and their potential applications: a review. *Adv. Funct. Mater.* **2016**, *26*, 1678−1698.

(3) Lim, H. R.; Kim, H. S.; Qazi, R.; Kwon, Y. T.; Jeong, J. W.; Yeo, W. H. Advanced Soft Materials, Sensor Integrations, and Applications of Wearable Flexible Hybrid Electronics in Healthcare, Energy, and Environment. *Adv. Mater.* **2019**, No. 1901924.

(4) Gong, S.; Lai, D. T.; Wang, Y.; Yap, L. W.; Si, K. J.; Shi, Q.; Jason, N. N.; Sridhar, T.; Uddin, H.; Cheng, W. Tattoolike polyaniline microparticle-doped gold nanowire patches as highly durable wearable sensors. *ACS Appl. Mater. Interfaces* **2015**, *7*, 19700−19708.

(5) Muth, J. T.; Vogt, D. M.; Truby, R. L.; Mengüç, Y.; Kolesky, D. B.; Wood, R. J.; Lewis, J. A. Embedded 3D printing of strain sensors within highly stretchable elastomers. *Adv. Mater.* **2014**, *26*, 6307−6312.

(6) Lee, H.; Seong, B.; Moon, H.; Byun, D. Directly printed stretchable strain sensor based on ring and diamond shaped silver nanowire electrodes. *RSC Adv.* **2015**, *5*, 28379−28384.

(7) Lee, C.; Jug, L.; Meng, E. High strain biocompatible polydimethylsiloxane-based conductive graphene and multiwalled carbon nanotube nanocomposite strain sensors. *Appl. Phys. Lett.* **2013**, *102*, No. 183511.

(8) Amjadi, M.; Pichitpajongkit, A.; Lee, S.; Ryu, S.; Park, I. Highly Stretchable and Sensitive Strain Sensor Based on Silver Nanowire−Elastomer Nanocomposite. *ACS Nano* **2014**, *8*, 5154−5163.

(9) Le, M. Q.; Ganet, F.; Audigier, D.; Capsal, J.-F.; Cottinet, P.-J. Printing of microstructure strain sensor for structural health monitoring. *Appl. Phys. A* **2017**, *123*, 354.

(10) Pan, T.; Pharr, M.; Ma, Y.; Ning, R.; Yan, Z.; Xu, R.; Feng, X.; Huang, Y.; Rogers, J. A. Experimental and theoretical studies of serpentine interconnects on ultrathin elastomers for stretchable electronics. *Adv. Funct. Mater.* **2017**, *27*, No. 1702589.

(11) Zymelka, D.; Yamashita, T.; Takamatsu, S.; Itoh, T.; Kobayashi, T. Printed strain sensor with temperature compensation and its evaluation with an example of applications in structural health monitoring. *Jpn. J. Appl. Phys.* **2017**, *56*, No. 05EC02.

(12) Ma, J.; Wang, P.; Chen, H.; Bao, S.; Chen, W.; Lu, H. Highly sensitive and large-range strain sensor with a self-compensated two-order structure for human motion detection. *ACS Appl. Mater. Interfaces* **2019**, *11*, 8527−8536.

(13) Wang, X.; Li, J.; Song, H.; Huang, H.; Gou, J. Highly stretchable and wearable strain sensor based on printable carbon nanotube layers/polydimethylsiloxane composites with adjustable sensitivity. *ACS Appl. Mater. Interfaces* **2018**, *10*, 7371−7380.

(14) Liu, S.; Zheng, R.; Chen, S.; Wu, Y.; Liu, H.; Wang, P.; Deng, Z.; Liu, L. A compliant, self-adhesive and self-healing wearable hydrogel as epidermal strain sensor. *J. Mater. Chem. C* **2018**, *6*, 4183−4190.

(15) Wan, S.; Zhu, Z.; Yin, K.; Su, S.; Bi, H.; Xu, T.; Zhang, H.; Shi, Z.; He, L.; Sun, L. A Highly Skin-Conformal and Biodegradable Graphene-Based Strain Sensor. *Small Methods* **2018**, *2*, No. 1700374.

(16) Lee, G.-Y.; Kim, M.-S.; Yoon, H.-S.; Yang, J.; Ihn, J.-B.; Ahn, S.-H. Direct printing of strain sensors via nanoparticle printer for the applications to composite structural health monitoring. *Procedia CIRP* **2017**, *66*, 238−242.

(17) Yin, F.; Ye, D.; Zhu, C.; Qiu, L.; Huang, Y. Stretchable, highly durable ternary nanocomposite strain sensor for structural health monitoring of flexible aircraft. *Sensors* **2017**, *17*, 2677.

(18) Borghetti, M.; Cantù, E. In *Preliminary Study on a Strain Sensor Printed on 3D-plastic Surfaces for Smart Devices*, 2019 II Workshop on Metrology for Industry 4.0 and IoT (MetroInd4.0 & IoT); IEEE, 2019; pp 249−253.

(19) Borghetti, M.; Serpelloni, M.; Sardini, E. Printed Strain Gauge on 3D and Low-Melting Point Plastic Surface by Aerosol Jet Printing and Photonic Curing. *Sensors* **2019**, *19*, 4220.

(20) Zhao, D.; Liu, T.; Zhang, M.; Liang, R.; Wang, B. Fabrication and characterization of aerosol-jet printed strain sensors for multifunctional composite structures. *Smart Mater. Struct.* **2012**, *21*, No. 115008.

(21) Wang, L.; Loh, K. J.; Mousacohen, R.; Chiang, W.-H. In *Printed Graphene-Based Strain Sensors for Structural Health Monitoring*, ASME2017 Conference on Smart Materials, Adaptive Structures and Intelligent Systems, American Society of Mechanical Engineers Digital Collection; ASME, 2017.

(22) Pegan, J. D.; Zhang, J.; Chu, M.; Nguyen, T.; Park, S.-J.; Paul, A.; Kim, J.; Bachman, M.; Khine, M. Skin-mountable stretch sensor for wearable health monitoring. *Nanoscale* **2016**, *8*, 17295−17303.

(23) Heo, Y.; Hwang, Y.; Jung, H. S.; Choa, S. H.; Ko, H. C. Secondary Sensitivity Control of Silver-Nanowire-Based Resistive-Type Strain Sensors by Geometric Modulation of the Elastomer Substrate. *Small* **2017**, *13*, No. 1700070.

(24) Agarwala, S.; Goh, G. L.; Dinh Le, T.-S.; An, J.; Peh, Z. K.; Yeong, W. Y.; Kim, Y.-J. Wearable bandage-based strain sensor for home healthcare: combining 3D aerosol jet printing and laser sintering. *ACS Sens.* **2018**, *4*, 218−226.

(25) Pang, C.; Koo, J. H.; Nguyen, A.; Caves, J. M.; Kim, M. G.; Chortos, A.; Kim, K.; Wang, P. J.; Tok, J. B. H.; Bao, Z. Highly skin-conformal microhairy sensor for pulse signal amplification. *Adv. Mater.* **2015**, *27*, 634−640.

(26) Drotlef, D. M.; Amjadi, M.; Yunusa, M.; Sitti, M. Bioinspired composite microfibers for skin adhesion and signal amplification of wearable sensors. *Adv. Mater.* **2017**, *29*, No. 1701353.

(27) Liu, X.; Liu, J.; Wang, J.; Wang, T.; Jiang, Y.; Hu, J.; Liu, Z.; Chen, X.; Yu, J. Bio-inspired, Micro-structured Silk Fibroin Adhesives for Flexible Skin Sensors. *ACS Appl. Mater. Interfaces* **2020**, *12*, 5601−5609.

(28) Liu, S.; Li, L. Ultrastretchable and self-healing double-network hydrogel for 3D printing and strain sensor. *ACS Appl. Mater. Interfaces* **2017**, *9*, 26429−26437.
(29) Xu, J.; Wang, G.; Wu, Y.; Ren, X.; Gao, G. Ultrastretchable Wearable Strain and Pressure Sensors Based on Adhesive, Tough, and Self-healing Hydrogels for Human Motion Monitoring. *ACS Appl. Mater. Interfaces* **2019**, *11*, 25613−25623.
(30) Xia, S.; Song, S.; Jia, F.; Gao, G. A flexible, adhesive and self-healable hydrogel-based wearable strain sensor for human motion and physiological signal monitoring. *J. Mater. Chem. B* **2019**, *7*, 4638−4648.
(31) Lv, R.; Bei, Z.; Huang, Y.; Chen, Y.; Zheng, Z.; You, Q.; Zhu, C.; Cao, Y. Mussel-Inspired Flexible, Wearable, and Self-Adhesive Conductive Hydrogels for Strain Sensors. *Macromol. Rapid Commun.* **2020**, *41*, No. 1900450.
(32) Rahman, M. T.; Moser, R.; Zbib, H. M.; Ramana, C.; Panat, R. 3D printed high performance strain sensors for high temperature applications. *J. Appl. Phys.* **2018**, *123*, No. 024501.
(33) Siddique, S.; Park, J. G.; Andrei, P.; Liang, R. M3D aerosol jet printed buckypaper multifunctional sensors for composite structural health monitoring. *Results Phys.* **2019**, *13*, No. 102094.
(34) Zhang, Y.; Anderson, N.; Bland, S.; Nutt, S.; Jursich, G.; Joshi, S. All-printed strain sensors: Building blocks of the aircraft structural health monitoring system. *Sens. Actuators, A* **2017**, *253*, 165−172.
(35) Lee, G.-Y.; Kim, M.-S.; Min, S.-H.; Kim, H.-S.; Kim, H.-J.; Keller, R.; Ihn, J.-B.; Ahn, S.-H. Highly Sensitive Solvent-free Silver Nanoparticle Strain Sensors with Tunable Sensitivity Created Using an Aerodynamically Focused Nanoparticle Printer. *ACS Appl. Mater. Interfaces* **2019**, *11*, 26421−26432.
(36) Farcau, C.; Moreira, H.; Viallet, B.; Grisolia, J.; Ciuculescu-Pradines, D.; Amiens, C.; Ressier, L. Monolayered wires of gold colloidal nanoparticles for high-sensitivity strain sensing. *J. Phys. Chem. C* **2011**, *115*, 14494−14499.
(37) Ketelsen, B.; Yesilmen, M.; Schlicke, H.; Noei, H.; Su, C.-H.; Liao, Y.-C.; Vossmeyer, T. Fabrication of Strain Gauges via Contact Printing: A Simple Route to Healthcare Sensors Based on Cross-Linked Gold Nanoparticles. *ACS Appl. Mater. Interfaces* **2018**, *10*, 37374−37385.
(38) Kim, H.; Lee, S.-W.; Joh, H.; Seong, M.; Lee, W. S.; Kang, M. S.; Pyo, J. B.; Oh, S. J. Chemically designed metallic/insulating hybrid nanostructures with silver nanocrystals for highly sensitive wearable pressure sensors. *ACS Appl. Mater. Interfaces* **2018**, *10*, 1389−1398.
(39) Herbert, R.; Mishra, S.; Lim, H. R.; Yoo, H.; Yeo, W. H. Fully Printed, Wireless, Stretchable Implantable Biosystem toward Battery-less, Real-Time Monitoring of Cerebral Aneurysm Hemodynamics. *Adv. Sci.* **2019**, *6*, No. 1901034.
(40) Mishra, S.; Kim, Y.-S.; Intarasirisawat, J.; Kwon, Y.-T.; Lee, Y.; Mahmood, M.; Lim, H.-R.; Herbert, R.; Yu, K. J.; Ang, C. S.; Yeo, W.-H. Soft, wireless periocular wearable electronics for real-time detection of eye vergence in a virtual reality toward mobile eye therapies. *Sci. Adv.* **2020**, *6*, No. eaay1729.
(41) Tu, L.; Yuan, S.; Zhang, H.; Wang, P.; Cui, X.; Wang, J.; Zhan, Y.-Q.; Zheng, L.-R. Aerosol jet printed silver nanowire transparent electrode for flexible electronic application. *J. Appl. Phys.* **2018**, *123*, No. 174905.
(42) Ali, M. M.; Maddipatla, D.; Narakathu, B. B.; Chlaihawi, A. A.; Emamian, S.; Janabi, F.; Bazuin, B. J.; Atashbar, M. Z. Printed strain sensor based on silver nanowire/silver flake composite on flexible and stretchable TPU substrate. *Sens. Actuators, A* **2018**, *274*, 109−115.
(43) Lee, J.; Lee, P.; Lee, H.; Lee, D.; Lee, S. S.; Ko, S. H. Very long Ag nanowire synthesis and its application in a highly transparent, conductive and flexible metal electrode touch panel. *Nanoscale* **2012**, *4*, 6408−6414.
(44) Hong, S.; Lee, H.; Yeo, J.; Ko, S. H. Digital selective laser methods for nanomaterials: From synthesis to processing. *Nano Today* **2016**, *11*, 547−564.
(45) Garnett, E. C.; Cai, W.; Cha, J. J.; Mahmood, F.; Connor, S. T.; Christoforo, M. G.; Cui, Y.; McGehee, M. D.; Brongersma, M. L. Self-limited plasmonic welding of silver nanowire junctions. *Nat. Mater.* **2012**, *11*, 241−249.
(46) Kim, Y. S.; Mahmood, M.; Lee, Y.; Kim, N. K.; Kwon, S.; Herbert, R.; Kim, D.; Cho, H. C.; Yeo, W. H. All-in-One, Wireless, Stretchable Hybrid Electronics for Smart, Connected, and Ambulatory Physiological Monitoring. *Adv. Sci.* **2019**, *6*, No. 1900939.
(47) Lee, Y.; Nicholls, B.; Lee, D. S.; Chen, Y.; Chun, Y.; Ang, C. S.; Yeo, W.-H. Soft electronics enabled ergonomic human-computer interaction for swallowing training. *Sci. Rep.* **2017**, *7*, No. 46697.
(48) Mishra, S.; Norton, J. J.; Lee, Y.; Lee, D. S.; Agee, N.; Chen, Y.; Chun, Y.; Yeo, W.-H. Soft, conformal bioelectronics for a wireless human-wheelchair interface. *Biosens. Bioelectron* **2017**, *91*, 796−803.
(49) Fan, J. A.; Yeo, W.-H.; Su, Y.; Hattori, Y.; Lee, W.; Jung, S.-Y.; Zhang, Y.; Liu, Z.; Cheng, H.; Falgout, L. Fractal design concepts for stretchable electronics. *Nat. Commun.* **2014**, *5*, No. 3266.
(50) Lee, S.; Amjadi, M.; Pugno, N.; Park, I.; Ryu, S. Computational analysis of metallic nanowire-elastomer nanocomposite based strain sensors. *AIP Adv.* **2015**, *5*, No. 117233.
(51) Choi, J. H.; Shin, M. G.; Jung, Y.; Kim, D. H.; Ko, J. S. Fabrication and Performance Evaluation of Highly Sensitive Flexible Strain Sensors with Aligned Silver Nanowires. *Micromachines* **2020**, *11*, 156.
(52) Kim, K. K.; Hong, S.; Cho, H. M.; Lee, J.; Suh, Y. D.; Ham, J.; Ko, S. H. Highly sensitive and stretchable multidimensional strain sensor with prestrained anisotropic metal nanowire percolation networks. *Nano Lett.* **2015**, *15*, 5240−5247.
(53) Li, J.; Zhao, S.; Zeng, X.; Huang, W.; Gong, Z.; Zhang, G.; Sun, R.; Wong, C.-P. Highly stretchable and sensitive strain sensor based on facilely prepared three-dimensional graphene foam composite. *ACS Appl. Mater. Interfaces* **2016**, *8*, 18954−18961.
(54) Lu, Y.; Biswas, M. C.; Guo, Z.; Jeon, J.-W.; Wujcik, E. K. Recent developments in bio-monitoring via advanced polymer nanocomposite-based wearable strain sensors. *Biosens. Bioelectron.* **2019**, *123*, 167−177.
(55) Zhao, Y.; Huang, X. Mechanisms and materials of flexible and stretchable skin sensors. *Micromachines* **2017**, *8*, 69.
(56) Gong, S.; Lai, D. T.; Su, B.; Si, K. J.; Ma, Z.; Yap, L. W.; Guo, P.; Cheng, W. Highly Stretchy Black Gold E-Skin Nanopatches as Highly Sensitive Wearable Biomedical Sensors. *Adv. Electron. Mater.* **2015**, *1*, No. 1400063.
(57) Song, Y. X.; Xu, W. M.; Rong, M. Z.; Zhang, M. Q. A sunlight self-healable transparent strain sensor with high sensitivity and durability based on a silver nanowire/polyurethane composite film. *J. Mater. Chem. A* **2019**, *7*, 2315−2325.
(58) Amjadi, M.; Yoon, Y. J.; Park, I. Ultra-stretchable and skin-mountable strain sensors using carbon nanotubes−Ecoflex nanocomposites. *Nanotechnology* **2015**, *26*, No. 375501.
(59) Hempel, M.; Nezich, D.; Kong, J.; Hofmann, M. A novel class of strain gauges based on layered percolative films of 2D materials. *Nano Lett.* **2012**, *12*, 5714−5718.
(60) Kim, Y.-S.; Basir, A. B.; Herbert, R.; Kim, J.; Yoo, H.; Yeo, W.-H. Soft Materials, Stretchable Mechanics, and Optimized Designs for Body-Wearable Compliant Antennas. *ACS Appl. Mater. Interfaces* **2019**, *12*, 3059−3067.
(61) Zhang, Y.; Xu, S.; Fu, H.; Lee, J.; Su, J.; Hwang, K.-C.; Rogers, J. A.; Huang, Y. Buckling in serpentine microstructures and applications in elastomer-supported ultra-stretchable electronics with high areal coverage. *Soft Matter* **2013**, *9*, 8062−8070.
(62) Jeong, Y. R.; Kim, J.; Xie, Z.; Xue, Y.; Won, S. M.; Lee, G.; Jin, S. W.; Hong, S. Y.; Feng, X.; Huang, Y.; Rogers, J. A.; Ha, J. S. A skin-attachable, stretchable integrated system based on liquid GaInSn for wireless human motion monitoring with multi-site sensing capabilities. *NPG Asia Mater.* **2017**, *9*, e443.
(63) Shakeel, M.; Khan, W. A.; Rahman, K. Fabrication of cost effective and high sensitivity resistive strain gauge using DIW technique. *Sens. Actuators, A* **2017**, *258*, 123−130.
(64) Yeo, W. H.; Kim, Y. S.; Lee, J.; Ameen, A.; Shi, L.; Li, M.; Wang, S.; Ma, R.; Jin, S. H.; Kang, Z. Multifunctional epidermal electronics printed directly onto the skin. *Adv. Mater.* **2013**, *25*, 2773−2778.
(65) Dai, S.; Zhao, J.; He, M.-r.; Wang, X.; Wan, J.; Shan, Z.; Zhu, J. Elastic properties of GaN nanowires: Revealing the influence of planar defects on Young's modulus at nanoscale. *Nano Lett.* **2015**, *15*, 8−15.

https://dx.doi.org/10.1021/acsami.0c04857
ACS Appl. Mater. Interfaces 2020, 12, 25020−25030

(66) Vivekchand, S.; Ramamurty, U.; Rao, C. Mechanical properties of inorganic nanowire reinforced polymer−matrix composites. *Nanotechnology* **2006**, *17*, S344.
(67) Wang, S.; Li, M.; Wu, J.; Kim, D.-H.; Lu, N.; Su, Y.; Kang, Z.; Huang, Y.; Rogers, J. A. Mechanics of epidermal electronics. *J. Appl. Mech.* **2012**, *79*, No. 527.
(68) Park, M.; Kim, M.-S.; Park, Y.-K.; Ahn, J.-H. Si membrane based tactile sensor with active matrix circuitry for artificial skin applications. *Appl. Phys. Lett.* **2015**, *106*, No. 043502.
(69) Dellon, E. S.; Mourey, R.; Dellon, A. L. Human pressure perception values for constant and moving one-and two-point discrimination. *Plast. Reconstr. Surg.* **1992**, *90*, 112−117.
(70) Kaneko, A.; Asai, N.; Kanda, T. The influence of age on pressure perception of static and moving two-point discrimination in normal subjects. *J. Hand Ther.* **2005**, *18*, 421−425.
(71) Ajovalasit, A.; Zuccarello, B. Local reinforcement effect of a strain gauge installation on low modulus materials. *J. Strain Anal. Eng. Des.* **2005**, *40*, 643−653.
(72) Ajovalasit, A.; D'Acquisto, L.; Fragapane, S.; Zuccarello, B. Stiffness and reinforcement effect of electrical resistance strain gauges. *Strain* **2007**, *43*, 299−305.
(73) Kim, Y.-S.; Mahmood, M.; Kwon, S.; Maher, K.; Kang, J. W.; Yeo, W.-H. Wireless, skin-like membrane electronics with multifunctional ergonomic sensors for enhanced pediatric care. *IEEE Trans. Biomed. Eng.* **2020**, No. 2956048.
(74) Yang, T.; Jiang, X.; Zhong, Y.; Zhao, X.; Lin, S.; Li, J.; Li, X.; Xu, J.; Li, Z.; Zhu, H. A wearable and highly sensitive graphene strain sensor for precise home-based pulse wave monitoring. *ACS Sens.* **2017**, *2*, 967−974.
(75) Martínez, G.; Howard, N.; Abbott, D.; Lim, K.; Ward, R.; Elgendi, M. Can photoplethysmography replace arterial blood pressure in the assessment of blood pressure? *J. Clin. Med.* **2018**, *7*, 316.

https://dx.doi.org/10.1021/acsami.0c04857
ACS Appl. Mater. Interfaces 2020, 12, 25020−25030